Published in final edited form as:
Biochemistry. 2011 December 13; 50(49): 10647–10657. doi:10.1021/bi201619z.

Binding of 3,4,5,6-tetrahydroxyazepanes to the acid-β-glucosidase active site: implications for pharmacological chaperone design for Gaucher disease†

Susan. D. Orwig[1], **Yun Lei Tan**[2], **Neil P. Grimster**[2], **Zhanqian Yu**[2], **Evan Powers**[2], **Jeffery W. Kelly**[2], and **Raquel L. Lieberman**[1,*]

[1]School of Chemistry & Biochemistry, Georgia Institute of Technology

[2]Skaggs Institute for Chemical Biology, Departments of Chemistry and Molecular and Experimental Medicine, The Scripps Research Institute

Abstract

Pharmacological chaperoning is a therapeutic strategy being developed to restore cellular folding and trafficking defects associated with Gaucher disease, a lysosomal storage disorder caused by point mutations in the gene encoding for acid- β-glucosidase (GCase). In this approach, small molecules bind to and stabilize mutant GCase in the endoplasmic reticulum (ER), increasing the concentration of folded, functional GCase trafficked to the lysosome where the mutant enzyme can hydrolyze accumulated substrate. To date, pharmacologic chaperone (PC) candidates investigated have largely been active-site-directed inhibitors of GCase, usually containing five- or six-membered rings, such as modified azasugars. Here we show that a seven-membered, nitrogen-containing heterocycle (3,4,5,6-tetrahydroxyazepane) scaffold is also promising for generating PCs for GCase. Crystal structures reveal that the core azepane stabilizes GCase in a variation of its proposed active conformation, whereas binding of an analog with an N-linked hydroxyethyl tail stabilizes a conformation of GCase in which the active site is covered, also utilizing a loop conformation not seen previously. Although both compounds preferentially stabilize GCase to thermal denaturation at pH 7.4, reflective of the pH in the ER, only the core azepane, which is a micromolar competitive inhibitor, elicits a modest increase in enzyme activity for the neuronopathic G202R- and the non-neuronopathic N370S- mutant GCase in an intact cell assay. Our results emphasize the importance of the conformational variability of the GCase active site in the design of competitive inhibitors as PCs for Gaucher disease.

Gaucher disease (GD), the most common lysosomal storage disorder (LSD), is caused by inherited point mutations in acid-β-glucosidase (GCase), a lysosomal enzyme that hydrolyzes glucosylceramide (GlcCer) (Fig. 1) as its main substrate (1). GCase mutations are not localized to its active site (2, 3). Rather, variants exhibit defects in protein stability (4) and cellular trafficking defects (5) leading to endoplasmic reticulum (ER) retention (6) and/or ER-associated degradation (ERAD) (7, 8), and accumulation of GlcCer and related substrates in the lysosome. Clinically, organomegalies, a weakened skeleton, and in severe

†Funding information: This work was sponsored by NIH F32AG027647, Blanchard Foundation, and Pew Foundation to R. L. L. S.D.O. was supported in part by United States Department of Education Graduate Assistance in Areas of National Need program P200A060188. Use of the APS was supported by the U. S. DOE, Office of Science, Office of Basic Energy Sciences, under Contract No. W-31-109-Eng-38.

*Correspondence: Raquel L. Lieberman, Ph. D., 901 Atlantic Drive NW, Atlanta, GA 30332-0400. Phone: (404) 385-3663, fax: (404) 894-2295, raquel.lieberman@chemistry.gatech.edu.

Supporting Information Available includes Supporting Fig. S1 and Fig. S2, which are available free of charge via the internet at http://pubs.acs.org.

cases, central nervous system (CNS) complications are observed (1, 9). Enzyme replacement (10) and substrate reduction therapy (SRT) (11–13) are expensive (14), if rather successful treatments for non-neuronopathic (Type 1) GD patients, but there is no treatment for neuronopathic GD, the most prevalent form of the disease worldwide (15). The emerging pharmacological chaperone (PC) therapeutic strategy proposes to use a small molecule to stabilize endogenous mutant GCase enzyme in the ER to allow more mutant GCase to engage its trafficking receptor, LIMP-2 (16). An increase in the concentration of GCase in the lysosome would then turn over substrate and mitigate clinical symptoms. PCs hold promise particularly for the treatment of neuronopathic GD variants because small molecules are likely to cross the blood-brain barrier (10), but also may be attractive in terms of cost to help overcome worldwide accessibility issues.

The desirable properties of PCs include high binding selectivity and affinity for the folded or near-folded enzyme conformations to increase the competent enzyme pool for trafficking and turnover. Somewhat paradoxically, the best PC candidates for GCase are noncovalent active site directed inhibitors, but because GCase has several close relatives in vivo, selective binding among closely-related enzymes has been an ongoing challenge (17, 18). Non-active site directed binders for GCase are still in the early stages of development (19, 20). One class of active site directed PC molecules for GCase is the deoxynojirimycins (DNJs, Fig. 1), first identified for SRT as an inhibitor of glucosylceramide synthase (17). N-butyl-deoxynojirimycin (NB-DNJ) exhibited weak chaperoning of mutant GCase in cell culture (21, 22), and a related analog, *N*-(*n*-nonyl)deoxynojirimycin (NN-DNJ), with a 10-fold lower half maximal inhibitory concentration (IC_{50}), was capable of chaperoning one of the two most prevalent GCase variants, namely the non-neuronopathic variant N370S, but not the neuronopathic variant L444P (22). Issues of enzyme selectivity (18) of DNJ analogs and toxicity (23) linger and these compounds have not been tested in human clinical trials (24). Other compounds such as cyclic-fused NJ hybrids (25–28), iminoxylitols (29), N-substituted δ-lactams (30), imino D-glucitols (22, 31), N-octyl-β-valienamine (NOV) (32, 33), aminocyclitols (34–36), the non-sugar Ambroxyl, an FDA-approved drug for an unrelated ailment (8, 37), and quinazoline analogues (38), are under investigation as PCs for GD, but are not yet progressing through clinical trials. Until recently, the leading clinical candidate had been isofagomine (Fig. 1; IFG, Plicera), an active-site-directed (39) and selective (40) iminosugar product analog, with a low nanomolar IC_{50}. IFG chaperones N370S- (41) and L444P- (40) mutant GCase in cell culture. Unfortunately, although the drug was well tolerated, clinical trials were halted after Phase 2 in 2009 because of the lack of therapeutic effect (42), which might be due to high dosing or off-target effects, among many other possibilities (43).

Optimism for the PC approach remains high, but the example of IFG illustrates the complexities in design, development, and clinical application of a therapeutic GCase pharmacologic chaperone. In spite of a body of design and synthesis of candidate PCs for mutant GCase, their characterization in vitro, in patient derived cell lines, and in some cases in animal models, the characteristics that make a PC a good clinical candidate remain poorly understood. We therefore have been seeking new PC scaffolds for GCase. In this study, we synthesized and characterized three GCase active-site-directed 3,4,5,6-tetrahydroxyazepane inhibitors (**1–3**; Fig. 1) that exhibit IC_{50} values in the low millimolar to micromolar range, a reasonable starting point for structure-based design. While the synthesis of polyhydroxylated seven-membered ring structures has been known for over 40 years (44), these analogs have only recently been explored as inhibitors of commercially available (45–51) or human (52, 53) glycosidases. Prior studies have not included GCase, and no analogs previously synthesized contain alkyl ether substructures attached to the endocyclic nitrogen like the inhibitors described herein. Our results demonstrate significant plasticity in the active site of GCase and its importance in the design of active site directed inhibitors as PCs for GD.

Experimental Procedures

Synthesis of Compounds 1, 2, and 3- (1*R*,1'*R*)-1,1'-((4*R*,5*R*)-2,2-dimethyl-1,3-dioxolane-4,5-diyl)bis(ethane-1,2-diol) (S-1)

2,2'-Dimethoxypropane (300 mL) was charged to a 1 L round bottom flask. D-Mannitol (20 g, 0.11 mol) and pyridinium *p*-toluenesulfonate (1 mol%, 0.27 g, 2.0 mmol) were added, and the suspension was stirred at reflux. After 18 hours, the solution was allowed to cool to room temperature and concentrated under reduced pressure. The residue was dissolved in ethyl acetate (300 mL) and washed with water (2 × 100 mL) and brine (100 mL). The organic layer was taken, dried over $MgSO_4$, filtered and evaporated under reduced pressure. The resultant white solid was charged to a 1 L round bottom flask. Acetic acid (210 mL) and water (90 mL) were added and the suspension was stirred at 40 °C. After 2 hours, the mixture was concentrated under reduced pressure. The residue was suspended in acetone (100 mL) and stirred at room temperature. After 1 hour, the mixture was filtered and the filtrate was concentrated under reduced pressure to yield **S-1** as a white solid (17.1g, 70 %). ^{1}H NMR (300 MHz, $CDCl_3$) δ ppm 4.17–4.23 (m, 2H), 3.90–4.05 (m, 2H), 3.70–3.77 (m, 4H), 1.45 (s, 6H); LCMS *m/z* 245.2 $[M + Na]^+$, calculated for $C_9H_{18}NaO_6^+$ 245.1. Data are consistent with literature (54).

(1*R*,1'*R*)-((4*S*,5*S*)-2,2-dimethyl-1,3-dioxolane-4,5-diyl)bis(2-((*tert*-butyldimethylsilyl)oxy)ethane -1,1-diyl) bis(4-methylbenzenesulfonate) (S-2)

S-1 (7.5 g, 33.8 mmol) was charged to a 500 mL round bottom flask under a nitrogen atmosphere. Anhydrous DMF (200 mL), imidazole (7.0 g, 100 mmol) and DMAP (0.16 g, 1.3 mmol) were added and the reaction was stirred at 0 °C. After 10 minutes, TBSCl (10.1 g, 68.0 mmol) was added portionwise and the solution was allowed to warm to room temperature. After 18 hours, the reaction mixture was diluted with ether/hexane (1:1, 500 mL), washed with water (3 × 100 mL), dried over $MgSO_4$ and concentrated under reduce pressure. Purification by flash column chromatography (silica, 9:1 hexane/ethyl acetate) afforded a colorless oil (8.0 g, 52 %). A sample (6.82 g, 15.15 mmol) was charged to a 500 mL round bottom flask. Anhydrous DCM (200 mL), DMAP (7.39 g, 60.5 mmol) and tosyl chloride were added and the mixture was stirred at room temperature. After 18 hours, the reaction was diluted with ethyl acetate (200 mL), washed with water (100 mL), aq. HCl (1 M, 100 mL), sat. aq. $NaHCO_3$ (100 mL) and brine (100 mL). The organic layer was taken dried over $MgSO_4$, filtered and concentrated under reduced pressure to afford **S-2** (10.0 g, 87 %) as a white solid. ^{1}H NMR (300 MHz, $CDCl_3$) δ ppm 7.81 (d, *J* = 8.4 Hz, 4H), 7.29 (d, *J* = 8.4 Hz, 4H), 4.68–4.72 (m, 2H), 4.36–4.40 (m, 2H), 3.83 (dd, *J* = 11.6, 4.6 Hz, 2H) 3.74 (dd, *J* = 11.6, 5.1 Hz, 2H), 2.43 (s, 6H), 1.14 (s, 6H), 0.83 (s, 18H), 0.1 (s, 12 H); LCMS *m/z* 781.4 $[M + Na]^+$, calculated for $C_{35}H_{58}NaO_{10}S_2Si_2^+$ 781.3.

(4*R*,5*R*)-2,2-dimethyl-4,5-di((*S*)-oxiran-2-yl)-1,3-dioxolane (S-3)

S-2 (10.0 g, 13.2 mmol) was charged to a 500 mL round bottom flask. THF (250 mL) and TBAF (1M in THF, 29.0 mL, 29.0 mmol) were added and the mixture was stirred at room temperature. After 2 hours, the reaction was concentrated under reduced pressure and the residues dissolved in ether (100 mL) and washed with sat. aq. $MgSO_4$ (3 × 100 mL), dried over $MgSO_4$, filtered and concentrated under reduced pressure. The residue was dissolved in anhydrous THF (120 mL), sealed under a nitrogen atmosphere and cooled 0 °C. Sodium hydride (60 % dispersion in mineral oil, 2.11 g, 52.7 mmol) was added portionwise. After 1 hour, the reaction was quenched with ice water (50 mL), and extracted with ether (3 × 20 mL). The organic layers were combined, dried over $MgSO_4$, filtered and concentrated under reduced pressure. Purification by flash column chromatography (silica, 8:2 hexane/ethyl acetate) afforded **S-3** (1.5 g, 60 %) as a white solid. ^{1}H NMR (300 MHz, $CDCl_3$) δ ppm 3.86 (dd, *J* = 3.2, 1.6 Hz, 2H), 3.04–3.10 (m, 2H), 2.85 (dd, *J* = 5.2, 4.1 Hz, 2H), 2.74 (2H, *J* =

5.2, 2.6 Hz, 2H), 1.41 (s, 6H); LCMS *m/z* 209.0 $[M + Na]^+$, calculated for $C_9H_{14}NaO_4^+$ 209.0. Data are consistent with literature (55).

(3*S*,4*R*,5*R*,6*S*)-3,4,5,6-tetrahydroxyazepan-1-ium chloride (1)

S-3 (120 mg, 0.64 mmol) was charged to a 5 mL round bottom flask. Water (2 mL) and benzylamine (freshly distilled, 69 mg, 70 μL, 0.64 mmol) were added and the mixture stirred at 95 °C. After 2 hours, the reaction was cooled to room temperature and concentrated under reduced pressure. Purification by flash chromatography (silica, 1:1 ethyl acetate/hexane) yielded a white solid, which was charged to a 10 mL round bottom flask. Methanol (5 mL), palladium on carbon (10%, 60 mg) and ammonium formate (122 mg, 1.9 mmol) were added and the mixture stirred at 70 °C. After 2 hours, the reaction was cooled to room temperature and 1-heptene (1.86 g, 2.66 mL, 19.0 mmol) was charged to the vessel. After stirring at room temperature for 1 hour, the reaction was filtered through celite, and evaporated under reduced pressure. The residue was dissolved in methanol (5 mL) and methanolic HCl (1 M, 5 mL, 5 mmol) was added. The mixture was stirred at room temperature. After 1 hour, the reaction was evaporated under reduced pressure to yield **1** as a gummy colorless solid (100 mg, 76 % from **S-3**). ^{1}H NMR (300 MHz, D_2O) δ ppm 4.06–4.18 (m, 2H), 3.69–3.76 (m, 2H), 3.34–3.44 (m, 2H), 3.18–3.30 (m, 2H); LCMS *m/z* 164.3 $[M + H]^+$, calculated for $C_6H_{14}NO_4^+$ 164.1. Data consistent with literature (55).

(3*S*,4*R*,5*R*,6*S*)-3,4,5,6-tetrahydroxy-1-(2-hydroxyethyl)azepan-1-ium chloride (2)

S-3 (120 mg, 0.64 mmol) was charged to a 5 mL round bottom flask. Water (2 mL) and ethanolamine (39 mg, 39 μL, 0.64 mmol) were added, and the mixture was stirred at 95 °C. After 2 hours, the reaction was cooled to room temperature and concentrated under reduced pressure. The residue was dissolved in methanol (5 mL) and methanolic HCl (1 M, 5 mL, 5 mmol) was added, and the mixture stirred at room temperature. After 1 hour, the reaction was evaporated under reduced pressure to yield **2** as a gummy yellow solid (144 mg, 93 %). ^{1}H NMR (300 MHz, D_2O) δ ppm 4.07–4.24 (m, 2H), 3.87–4.01 (m, 2H), 3.61–3.77 (m, 4H), 3.44–3.58 (m, 4H); LCMS *m/z* 208.2 $[M + H]^+$, calculated for $C_8H_{18}NO_4^+$ 208.1.

(3*S*,4*R*,5*R*,6*S*)-3,4,5,6-tetrahydroxy-1-(2-(2-hydroxyethoxy)ethyl)azepan-1-ium chloride (3)

S-3 (120 mg, 0.64 mmol) was charged to a 5 mL round bottom flask. Water (2 mL) and 2-(2-aminoethoxy)ethanol (67 mg, 64 μL, 0.64 mmol) were added and the mixture was stirred at 95 °C. After 2 hours, the reaction was cooled to room temperature and concentrated under reduced pressure. The residue was dissolved in methanol (5 mL) and methanolic HCl (1 M, 5 mL, 5 mmol) was added, and the mixture stirred at room temperature. After 1 hour, the reaction was concentrated under reduced pressure to yield **3** as a gummy yellow solid (174 mg, 95 %). ^{1}H NMR (300 MHz, D_2O) δ ppm 4.10–4.23 (m, 2H), 3.92–3.99 (m, 2H), 3.61–3.80 (m, 4H), 3.34–3.57 (m, 8H); LCMS *m/z* 208.1 $[M + H]^+$, calculated for $C_8H_{18}NO_4^+$ 208.1.

In vitro GCase inhibition assay

15 ng of Cerezyme® (Genzyme corp.) was mixed with McIlvaine buffer (0.1 M citrate, 0.2 M phosphate, pH 5.4), 0.1% Triton X-100, 0.25% taurochloric acid, and various concentrations of **1**, **2**, or **3** on ice. A stock of 300 mM 4-methylumbelliferyl-β-glucopyranoside (4MU-β-Glc, Sigma) was freshly prepared in dimethylsulfoxide (DMSO), and added to the Cerezyme/inhibitor mixture at a final concentration of 3 mM. The reaction was then transferred into a microplate (Grenier), sealed, and incubated at 37 °C for 30 minutes. An equal volume of 0.4 M glycine and 0.4 M NaOH was added to each well to quench the reaction. The release of 4-methylumbelliferone (4MU) was measured by fluorescence (excitation filter 360/40 nm, emission 460/40 nm) on a BioTek microplate

reader. Each reaction was set up in triplicate per plate, averaged, and background subtracted. Each plate was repeated in triplicate per inhibitor and the averaged, normalized data was plotted against drug concentration and fitted to a log(inhibitor) vs response-variable slope curve in GraphPad Prism to estimate the IC_{50}. To investigate the effect of incubation time of premixed inhibitor and enzyme, the Cerezyme/**2** mixture was incubated at 4 °C for 16 hours. 4MU- β-Glc was then added and the assay carried out as described above. An inhibition assay with IFG (Toronto Research Chemicals) was also carried out as a positive control with a result similar to that previously published (39).

Thermal stability assay for GCase

Cerezyme was resuspended in 0.1 M citrate, 0.2 M phosphate, adjusted either to pH 5.2 or pH 7.2, and protein concentration was determined via Bradford assay (56). A working stock of 10 μM Cerezyme was prepared by diluting in the appropriate buffer. Reactions of 30 μL were prepared at room temperature by diluting Cerezyme in water (1:10) along with various concentrations of inhibitor (0– 10 mM), also prepared in water. This resulted in a final buffer concentration of 0.01 M citrate, 0.02 M phosphate, either at pH 5.2 or 7.2, and 1 μM protein. Finally, Sypro Orange (Invitrogen, supplied as 5000X solution in DMSO) was diluted in water and then added to each reaction with a final concentration of 5X. Each reaction was delivered to 96-well optical plates (Applied Biosystems) before sealing with optical film. Fluorescence data were acquired on an Applied Biosciences Step-One Plus RT-PCR instrument equipped with a fixed excitation wavelength (480 nm) and a ROX emission filter (610 nm). Melts were conducted from 25–95 °C with a 1 °C per min increase. Collected data were baseline subtracted, trimmed to include both the boundaries and the transition of interest, and subjected to Boltzmann sigmoid analysis as described previously (57).

Intact cell GCase activity assay

The heterozygous Gaucher fibroblasts containing the N370S/V394L GC mutation (GM01607) were obtained from the Coriell Cell Repositories (Camden, NJ). Fibroblasts were grown in minimal essential medium with Earle's salts (supplemented with 10 % heat-inactivated fetal bovine serum and 1 % glutamine Pen-Strep at 37 °C in 5 % CO_2). Cell culture media were obtained from Gibco (Grand Island, NY). Briefly, cells were plated into 96-well plates (100 μL per well). After cell attachment, the media was replaced with fresh media containing small molecules and incubated at 37 °C for 3 days. The media was removed and cell monolayers washed with Dulbecco's phosphate buffered saline. The assay was started by the addition of 50 μl of 2.5 mM 4MU-β-Glc in 0.2 M acetate buffer (pH 4.0) to each well, followed by incubation at 37 °C for 1–4 hours. The extent of unspecific non-lysosomal GC activity was evaluated by adding CBE (Toronto Research Chemicals) to control wells. The reaction was stopped by the addition of 150 μL of 0.2 M glycine buffer (pH 10.8). Liberated 4MU was measured (excitation 365 nm, emission 445 nm) with a Molecular Devices SpectraMax Gemini fluorescence plate reader. Small molecules were assayed at least in triplicate at each concentration, and on three different days. Cells appeared intact when viewed under a light microscope. The data reported were normalized to the enzyme activity of cells of the same type treated with vehicle control (H_2O) and expressed as percentage of WT enzyme activity.

Crystallization, Data Collection, Structure Determination and Refinement

Cerezyme was concentrated to 3 mg/mL in 0.02% sodium azide, 10 mM citrate buffer, pH 5.5, and 7% (v/v) ethanol. Crystals of GCase were grown by vapor diffusion at room temperature using a cocktail composed of 11–12% PEG 3350, 0.18–0.205 M ammonium sulfate, and 0.1 M acetate buffer, pH 4.6. Crystals with **1** and **2** were generated by soaking crystals in the reservoir solution supplemented with 1 mM inhibitor for 5 minutes or 5 days,

respectively. Crystals were protected with 20% ethylene glycol and cryocooled in liquid N_2. Data were collected at the Southeast Regional Collaborative Access Team (SER-CAT) Beamlines at the Advanced Photon Source at Argonne National Labs (Darien, IL). Data sets were indexed and scaled using HKL2000 (58) and structures were solved by rigid body refinement in REFMAC5 (59) utilizing the asymmetric unit of just the GCase polypeptide (4 copies of GCase in asymmetric unit of PDB ID 2NSX) as the initial model. Compounds were identified by significant (> +3σ) $F_o - F_c$ difference Fourier density in the active site after initial rigid body refinement (Fig. 3). All four active site copies in the asymmetric unit were occupied with **1** whereas with **2**, like for IFG (39), only two of the four active site copies had bound ligand. For the protein, restrained refinement was performed against the highest resolution of the data with REFMAC5 (59) and model rebuilding with Coot (60). Models for **1** and **2** were generated using PRODRG (61) and figures generated using PyMOL (62). For both structures, 99% or better of the residues lie in the most favored and additionally allowed regions of the Ramachandran plot. Crystallographic statistics appear in Table 1 and coordinates have been deposited to the protein databank with PDB ID codes 3RIL (**1**) and 3RIK (**2**).

Results and Discussion

Inhibitor design and synthesis

To extend the previously studied 5-membered ring scaffolds and 6-membered ring glucose-derived PCs (4, 9, 22, 63), three 7-membered 3,4,5,6-tetrahydroxyazepane iminosugar analogs (**1–3**; Fig. 1) were synthesized as potential GCase inhibitors and PCs by procedures slightly modified from those reported in the literature (55) (see Schemes 1–3 and Experimental Procedures). We retained an endocyclic nitrogen because, depending on their binding orientation, protonated iminosugars and azasugars can mimic the glycosidase transition state (64). In addition, the increased number of substituents can be exploited in future drug efforts to tune the hydrogen bonding network to select against unwanted inhibition of other glucosidases, a known problem (18). Finally, instead of the straight alkyl chains used previously, alkyl ether tails were installed to assist in discriminating between anomeric carbon configurations (65), reduce the lipophilicity of the candidate PC, better match the polarity of the ceramide component of the substrate to the GCase binding site, and/or decrease the cytotoxicity reported for related compounds (17).

Inhibition profiles

The inhibitory activities of compounds **1**, **2**, and **3** toward GCase were determined using competition for the fluorogenic substrate 4MU-β-Glc (66). Compound **1** exhibited the strongest competitive inhibition, with an IC_{50} of 146 μM (Fig. 2a), comparable to DNJ (IC_{50}= 240 μM) and NB-DNJ (IC_{50}= 270 μM) (67) but 10-fold weaker than NN-DNJ (22) and 250-fold weaker than IFG (39). In contrast, compounds **2** and **3** exhibited weaker IC_{50} values of 3.4 mM and >15 mM, respectively (Fig. 2b, c). To address the possibility of slow binding kinetics, GCase was preincubated with **2** for 16 h prior to the addition of substrate. No change in the IC_{50} value was observed, suggesting that the on-rate is not slow (data not shown).

Stabilization to thermal denaturation

Since active-site inhibitors are likely to stabilize GCase against thermal denaturation, we measured the change in stability of GCase in the presence of inhibitor by differential scanning fluorimetry (DSF). Melting temperatures (T_ms) recorded for GCase using the low-volume and facile DSF method are within ~3 K of those reported by DSC using similar concentrations of enzyme and inhibitor, but with slightly different buffers (68). Comparison of the T_m values for GCase in the presence of the highest concentration of inhibitors reveals

only a 1–3 K increase in stability at acidic pH and a higher, 6–7.5 K increase at neutral pH (Table 2). Thus, while stabilization is modest compared to IFG (Table 2), all three compounds confer more stability to GCase at a neutral pH (reflective of the pH in the ER) than at the lower lysosomal pH, but stabilize GCase to the same extent as one another.

Structural characterization

Crystal structures of **1** and **2** bound to wild-type GCase were solved to 2.4 and 2.5 Å resolution (Table 1), whereas a structure with **3**, also the weakest binder, could not be obtained. Suitable quantities of mutant GCase were not available for crystallization trials, but the PC is designed to stabilize the near-folded state of the enzyme, which is expected to be the same for the wild-type and GD-causing missense variants. The global structure of GCase remains unchanged by ligand binding, but adjustments are seen in the active site and surrounding loop residues. Below, we focus on the relevant active site (Fig. 3), loop (Figs. 4, 5), and interior regions (Fig. 5) of GCase affected by binding of **1** and **2**, and compare the structures to previously solved GCase structures with two other well-studied candidate PC systems (69), namely, the product analog IFG (39) and DNJs (70).

In the GCase active site, both **1** and **2** bind and are held in place by a hydrogen bonding network (Fig. 3a, b). In the case of **2**, which is bound in a distorted chair conformation, the hydroxyl substituents at positions 3 and 4 (see Fig. 1) are equatorial and within hydrogen bonding distance of Asp 127, Trp 179, Asn 234, and Trp 381 side chains on GCase, whereas the likewise equatorial 6-hydroxyl moiety is not involved in any polar interactions (Fig. 3a). The main distortions from the chair conformation appear at positions 1 and 2, which face Asn 234 and Glu 235, the residue implicated as the general acid/base in catalysis (2, 71). Notably, the hydroxyl substituent at position 2 is restrained by a hydrogen bonding interaction with Asn 234 and from below, the catalytic nucleophile Glu 340 (72). Glu 340 is also within hydrogen bonding distance of the endocyclic nitrogen and hydroxyethyl tail; all three interactions with the Glu 340 carboxylate side chain are quite short, ~ 2.7 Å. By comparison, binding of **1** in the GCase active site appears less conformationally constrained. Similar interactions stabilize equatorial 3- and 4-hydroxyl arms of **1** in the GCase active site (Fig. 3b). An additional interaction of the 6-hydroxyl group with Tyr 313 is seen, and the 2-hydroxyl group appears less distorted, now within hydrogen bonding distance of Asn 234 only. This change in interactions with the hydroxyl group at position 2 may be a result of the conformationally mobile endocyclic nitrogen, which is not involved in any interactions with GCase (Fig. 3a,b). The resolution of this structure is insufficient to clarify the occupancy details of different puckered states of the ring, however. Interestingly, even though **2** is stabilized by more polar interactions than the less strained **1**, it is the weaker competitive inhibitor (see above).

The binding orientations of **1** and **2** are close to those found in NB-DNJ- and NN-DNJ- (Fig. 3c) bound GCase (70). First, neither our compounds nor the DNJs are hydrogen bonded to Glu 235. This is in contrast to IFG-bound GCase (Fig. 3d), where a likely deprotonated Glu 235 stabilizes the IFG imino group (39). Second, the positions of the endocyclic nitrogens of **1**, **2**, NB- and NN-DNJ are nearly superimposable, and shifted compared to IFG- bound GCase. However, in the case of NB- and NN-DNJ, the endocyclic nitrogens are held in place by a water-mediated hydrogen bond to the hydyroxyl group of Tyr 244; a corresponding water molecule was not resolved in either of our two structures. The preferential binding mode appears to derive from the interaction between the 3-hydroxyl group on the inhibitor and Asn 234 common to the DNJs, **1**, and **2** (Fig. 3), but not IFG. This observation could be exploited in future design to tune the product or transition state mimicking properties of the compound.

Notable differences in structure are observed in the active site loops (Loop 1: residues 311–319 and Loop 2: residues 342–354, Fig. 4) when comparing the binding modes of **1** (yellow) and **2** (orange) to each other and to previously reported GCase structures with bound IFG and DNJs (green and blue, respectively). The alterations, particularly in Loop 1, reinforce the notion that the conformational flexibility of GCase beyond the site of catalysis is an important consideration in the design of active-site binders as PCs. Although Loop 2 (residues 342–354) is also shifted 3.2 Å from its position in the IFG or glycerol (39) bound GCase structures (Supporting Fig. S1), these movements appear to be due to different crystal contacts used among the various GCase crystal forms; we observe the same orientation of Loop 2 is seen in apo GCase crystallized under the conditions used here for azepane inhibitor soaking (data not shown). By contrast, for Loop 1, highly relevant changes due to ligand binding are observed. On the basis of the IFG-bound structure, the helical Loop 1 has been proposed to be the catalytically active form of GCase (39). To date, has been observed only when a small molecule with reported chaperoning capabilities like the DNJ analogs (28, 70) or IFG (39), is bound to the GCase active site; extended Loop 1 has been seen with bound sulfate (71), glycerol (39), or the suicide inhibitor conduritol- β-epoxide (CBE) (73), and in the catalytically compromised N370S-mutant GCase structure at both neutral or acidic pH (74).

At first glance GCase adopts recognized Loop 1 structures, namely, extended over the catalytic center when **2** binds, and an α-helical arrangement (Fig. 4, Supporting Fig. S2) that exposes the active site when **1** is bound. However, each is distinct from conformations seen previously. For example, in other structures, the side chain of Tyr 313 is within hydrogen bonding distance of the carboxylate of Glu 235 when Loop 1 is extended (not shown), but switches to interacting with Glu 340 when Loop 1 is helical (see Fig. 5a). Although the expected helical Loop 1 Tyr 313 – Glu 340 interaction is seen when **1** is bound to GCase (Fig. 5b), the interaction with Tyr 313 for the extended Loop 1 when **2** binds, is not. The hydroxyethyl substituent on **2** replaces Tyr 313 in hydrogen bonding interactions with Glu 340 (Fig. 5c), which leads to a new water-mediated interaction between Tyr 313 and Asn 396 (Fig. 3a) that still caps the active site entrance. Second, in addition to changes near Tyr 313 in the site of catalysis, helical-turn stabilizing interactions of Loop 1 involving an interior helix of GCase have been altered when **1** is bound (Fig 5, bottom panels), leading to a more relaxed structure. For reference, in the NB-DNJ, NN-DNJ, and IFG structures (see IFG: Fig. 5a, bottom panel), Asp 315 in the helical Loop 1 forms a salt bridge with the guanidinium of Arg 285 (omitted in Fig. 5 for clarity) and is linked to Ser 366 and Asn 370 on the helix via a bound water molecule. Concurrently, the side chain of Trp 312 interacts with the carbonyl backbone of Cys 342, located on Loop 2 (69). Unexpectedly, in our structure with **1** bound, the side chain of Trp 312 is repositioned to form a new interaction with Ser 366 instead of Cys 342 (Fig. 5b, bottom panel). This interaction has only been seen once before, in the low pH structure of N370S-GCase (74), which retains ~ 30% catalytic activity *in vitro* (2) and where Loop 1 is extended. The Trp 312 – Ser 366 interaction serves to shift Asp 315 away from Arg 285 to a distance consistent with a hydrogen bonding interaction. This more relaxed Loop 1 configuration observed with **1** bound may at least in part explain for its weaker competitive inhibition compared to IFG or NN-DNJ.

Enhancement of cellular enzyme activity

To evaluate **1**, **2**, and **3** for PC activity, their abilities to enhance mutant GCase activity in an intact cell assay (22) were examined next. Patient-derived skin fibroblasts harboring either mutant G202R GCase (associated with the neuronopathic Type 2 GD) or mutant N370S/V394L GCase (associated with the non-neuronopathic Type 1 GD) were incubated with compounds **1**, **2**, or **3** for three days at varying concentrations. Based on cytotoxicity data from related compounds (17, 23), the upper limit tested was 100 μM. Compound **1** increased

the cellular GCase activity of G202R fibroblasts by 20% at 100 μM, whereas **2** and **3** had no effect on activity in the concentration range tested (Fig. 6a). A similar but attenuated result was obtained for N370S/V394L GCase fibroblasts. A ~15% increase in activity was observed for cells treated with 10 μM of **1** (Fig. 6b), a lower concentration than was required for a similar effect with G202R and comparable to the optimal concentration observed for NN-DNJ (22). The maximal 20% activity enhancement for G202R GCase is intermediate between no enhancement seen for NB-DNJ and 60–65% enhancement seen for NN-DNJ using the same enzyme variant and experimental setup (22), and is in the desired 10–15 % enzyme activity shown to reduce clinical manifestations in a related LSD (75) and thought to be a threshold of activity in the lysosome necessary to prevent GD symptoms (76). Thus, the modest increase in activity, while not sufficient to claim that **1** is a bona fide PC candidate for GCase, strongly suggests that the azepane ring system is a promising scaffold for future structure-based design efforts to develop novel PCs for GCase.

Conclusions

In this study, we synthesized N-linked hydroxyl alkyl and alkyl ether azepanes inhibitors **1–3** as potential PCs for GCase. The active site of GCase readily accommodates the larger 7-membered azepane ring, but the enzyme is exquisitely sensitive to binding and can propagate binding-induced conformational changes as far as ~ 13 Å away from the binding site, within the interior of the enzyme. Compounds **1–3** stabilize GCase against thermal denaturation to approximately the same extent and preferentially at neutral over acidic pH. However, only **1**, which exhibits a ~10x better competitive inhibition profile compared to **2** and **3**, exhibits any enhancement of enzyme activity in fibroblasts expressing G202R- and N370S-mutant GCase. Binding of **1** results in a helical arrangement of Loop 1, albeit one that is more relaxed than observed previous for IFG and DNJs (69). Notably, even though **2** generates a GCase loop conformation thought to be inactive, this compound does not exhibit a favorable chaperoning profile in cells. In sum, a link is emerging between competitive inhibition of GCase in vitro and the conformation of Loop 1 that exposes the GCase active site, with the ability to increase mutant GCase activity in cell culture. Thermal stabilization, a common feature of an inhibitor, is not a singular adequate predictor of cellular enzyme activity enhancement for GCase. In this regard, the core azepane **1** is a promising scaffold on which to build more potent competitive inhibitors as potential PCs. For example, inferred from comparison of crystal structures, the introduction of a 6-hydroxymethyl arm and removal of a 3-hydroxyl group, or introduction of unsaturated bonds (25, 26, 28) in **1** may shift binding to better mimic the transition state or product, and thereby generate a better competitive azepane inhibitor. It may also be possible to overcome some of the selectivity issues by taking advantage of the GCase active site plasticity, which may bind PC scaffolds that cannot be accommodated in related enzymes. Overall, we anticipate that biochemical studies of potential PCs with corresponding enzyme structures will continue to provide valuable insight into priorities for inhibitor design that will lead to the identification of compounds worthy of detailed cellular trafficking and animal model studies, and ultimately, to a successful outcome of clinical trials of a therapeutic PC for GD.

Supplementary Material

Refer to Web version on PubMed Central for supplementary material.

Abbreviations

GCase	acid- β-glucosidase
ER	endoplasmic reticulum

GD	Gaucher Disease
ERAD	ER-associated degradation
CNS	central nervous system
NB-DNJ	N-butyldeoxynojirimycin
NN-DNJ	*N*-(*n*-nonyl) deoxynojirimycin
GlcCer	glucosylceramide
SRT	substrate replacement therapy
PC	pharmacologic chaperone
IFG	isofagomine
4MU-β-Glc	4-methylumbelliferyl-β-glucopyranoside
DSF	differential scanning fluorimetry
DSC	differential scanning calorimetry
T_m	melting temperature
LSD	lysosomal storage disorder

References

1. Beutler E, Gelbart T. Glucocerebrosidase (Gaucher disease). Hum. Mutat. 1996; 8:207–213. [PubMed: 8889578]
2. Liou B, Kazimierczuk A, Zhang M, Scott CR, Hegde RS, Grabowski GA. Analyses of variant acid beta -glucosidases: effects of gaucher disease mutations. J. Biol. Chem. 2006; 281:4242–4253. [PubMed: 16293621]
3. Grace ME, Newman KM, Scheinker V, Berg-Fussman A, Grabowski GA. Analysis of human acid beta-glucosidase by site-directed mutagenesis and heterologous expression. J. Biol. Chem. 1994; 269:2283–2291. [PubMed: 8294487]
4. Sawkar AR, Schmitz M, Zimmer KP, Reczek D, Edmunds T, Balch WE, Kelly JW. Chemical chaperones and permissive temperatures alter localization of Gaucher disease associated glucocerebrosidase variants. ACS Chem. Biol. 2006; 1:235–251. [PubMed: 17163678]
5. Schmitz M, Alfalah M, Aerts JM, Naim HY, Zimmer KP. Impaired trafficking of mutants of lysosomal glucocerebrosidase in Gaucher's disease. Int. J. Biochem. Cell Biol. 2005; 37:2310–2320. [PubMed: 15982918]
6. Zimmer KP, le Coutre P, Aerts HM, Harzer K, Fukuda M, O'Brien JS, Naim HY. Intracellular transport of acid beta-glucosidase and lysosome-associated membrane proteins is affected in Gaucher's disease (G202R mutation). J. Pathol. 1999; 188:407–414. [PubMed: 10440752]
7. Ron I, Horowitz M. ER retention and degradation as the molecular basis underlying Gaucher disease heterogeneity. Hum. Mol. Genet. 2005; 14:2387–2398. [PubMed: 16000318]
8. Bendikov-Bar I, Ron I, Filocamo M, Horowitz M. Characterization of the ERAD process of the L444P mutant glucocerebrosidase variant. Blood Cells Mol. Dis. 2011; 46:4–10. [PubMed: 21106416]
9. Yu Z, Sawkar AR, Kelly JW. Pharmacologic chaperoning as a strategy to treat Gaucher disease. FEBS J. 2007; 274:4944–4950. [PubMed: 17894779]
10. Cox TM. Gaucher disease: clinical profile and therapeutic developments. Biologics. 2010; 4:299–313. [PubMed: 21209725]
11. Lee A, Abe A, Shayman JA. Improved inhibitors of glucosylceramide synthase. J. Biol. Chem. 1999; 274:14662–14669. [PubMed: 10329660]
12. Lukina E, Watman N, Arreguin EA, Banikazemi M, Dragosky M, Iastrebner M, Rosenbaum H, Phillips M, Pastores GM, Rosenthal DI, Kaper M, Singh T, Puga AC, Bonate PL, Peterschmitt MJ.

A phase 2 study of eliglustat tartrate (Genz-112638), an oral substrate reduction therapy for Gaucher disease type 1. Blood. 2010; 116:893–899. [PubMed: 20439622]

13. Lukina E, Watman N, Arreguin EA, Dragosky M, Iastrebner M, Rosenbaum H, Phillips M, Pastores GM, Kamath RS, Rosenthal DI, Kaper M, Singh T, Puga AC, Peterschmitt MJ. Improvement in hematological, visceral, and skeletal manifestations of Gaucher disease type 1 with oral eliglustat tartrate (Genz-112638) treatment: 2-year results of a phase 2 study. Blood. 2010; 116:4095–4098. [PubMed: 20713962]
14. Wraith JE. Limitations of enzyme replacement therapy: current and future. J. Inherit. Metab. Dis. 2006; 29:442–447. [PubMed: 16763916]
15. Michelakakis H, Skardoutsou A, Mathioudakis J, Moraitou M, Dimitriou E, Voudris C, Karpathios T. Early-onset severe neurological involvement and D409H homozygosity in Gaucher disease: outcome of enzyme replacement therapy. Blood Cells Mol. Dis. 2002; 28:1–4. [PubMed: 11814305]
16. Reczek D, Schwake M, Schroder J, Hughes H, Blanz J, Jin X, Brondyk W, Van Patten S, Edmunds T, Saftig P. LIMP-2 is a receptor for lysosomal mannose-6-phosphate-independent targeting of beta-glucocerebrosidase. Cell. 2007; 131:770–783. [PubMed: 18022370]
17. Butters TD, van den Broek LAGM, Fleet GWJ, Krulle TM, Wormald MR, Dwek RA, Platt FM. Molecular requirements of imino sugars for the selective control of N-linked glycosylation and glycosphingolipid biosynthesis. Tetrahedron: Asymmetry. 2000; 11:113–124.
18. Mellor HR, Neville DC, Harvey DJ, Platt FM, Dwek RA, Butters TD. Cellular effects of deoxynojirimycin analogues: inhibition of N-linked oligosaccharide processing and generation of free glucosylated oligosaccharides. Biochem. J. 2004; 381:867–875. [PubMed: 15128289]
19. Landon MR, Lieberman RL, Hoang QQ, Ju S, Caaveiro JM, Orwig SD, Kozakov D, Brenke R, Chuang GY, Beglov D, Vajda S, Petsko GA, Ringe D. Detection of ligand binding hot spots on protein surfaces via fragment-based methods: application to DJ-1 and glucocerebrosidase. J. Comput. Aided Mol. Des. 2009; 23:491–500.
20. Zheng W, Padia J, Urban DJ, Jadhav A, Goker-Alpan O, Simeonov A, Goldin E, Auld D, LaMarca ME, Inglese J, Austin CP, Sidransky E. Three classes of glucocerebrosidase inhibitors identified by quantitative high-throughput screening are chaperone leads for Gaucher disease. Proc. Natl. Acad. Sci. U S A. 2007; 104:13192–13197. [PubMed: 17670938]
21. Alfonso P, Pampin S, Estrada J, Rodriguez-Rey JC, Giraldo P, Sancho J, Pocovi M. Miglustat (NB-DNJ) works as a chaperone for mutated acid beta-glucosidase in cells transfected with several Gaucher disease mutations. Blood Cells Mol. Dis. 2005; 35:268–276. [PubMed: 16039881]
22. Sawkar AR, Cheng WC, Beutler E, Wong CH, Balch WE, Kelly JW. Chemical chaperones increase the cellular activity of N370S beta -glucosidase: a therapeutic strategy for Gaucher disease. Proc. Natl. Acad. Sci. U.S.A. 2002; 99:15428–15433. [PubMed: 12434014]
23. Chang HH, Asano N, Ishii S, Ichikawa Y, Fan JQ. Hydrophilic iminosugar active-site-specific chaperones increase residual glucocerebrosidase activity in fibroblasts from Gaucher patients. FEBS J. 2006; 273:4082–4092. [PubMed: 16934036]
24. Sawkar AR, D'Haeze W, Kelly JW. Therapeutic strategies to ameliorate lysosomal storage disorders--a focus on Gaucher disease. Cell. Mol. Life Sci. 2006; 63:1179–1192. [PubMed: 16568247]
25. Brumshtein B, Aguilar-Moncayo M, Garcia-Moreno MI, Ortiz Mellet C, Garcia Fernandez JM, Silman I, Shaaltiel Y, Aviezer D, Sussman JL, Futerman AH. 6-Amino6-deoxy-5,6-di-N-(N'-octyliminomethylidene)nojirimycin: synthesis, biological evaluation, and crystal structure in complex with acid beta-glucosidase. Chembiochem. 2009; 10:1480–1485. [PubMed: 19437524]
26. Luan Z, Higaki K, Aguilar-Moncayo M, Ninomiya H, Ohno K, Garcia-Moreno MI, Ortiz Mellet C, Garcia Fernandez JM, Suzuki Y. Chaperone activity of bicyclic nojirimycin analogues for Gaucher mutations in comparison with N-(n-nonyl)deoxynojirimycin. Chembiochem. 2009; 10:2780–2792. [PubMed: 19830760]
27. Aguilar-Moncayo M, Garcia-Moreno MI, Trapero A, Egido-Gabas M, Llebaria A, Fernandez JM, Mellet CO. Bicyclic (galacto)nojirimycin analogues as glycosidase inhibitors: effect of structural modifications in their pharmacological chaperone potential towards beta-glucocerebrosidase. Org. Biomol. Chem. 2011; 9:3698–3713. [PubMed: 21451818]

28. Brumshtein B, Aguilar-Moncayo M, Benito JM, Garcia Fernandez JM, Silman I, Shaaltiel Y, Aviezer D, Sussman JL, Futerman AH, Ortiz Mellet C. Cyclodextrin-mediated crystallization of acid beta-glucosidase in complex with amphiphilic bicyclic nojirimycin analogues. Org. Biomol. Chem. 2011; 9:4160–4167. [PubMed: 21483943]

29. Oulaidi F, Front-Deschamps S, Gallienne E, Lesellier E, Ikeda K, Asano N, Compain P, Martin OR. Second-generation iminoxylitol-based pharmacological chaperones for the treatment of Gaucher disease. ChemMedChem. 2011; 6:353–361. [PubMed: 21275057]

30. Wang GN, Reinkensmeier G, Zhang SW, Zhou J, Zhang LR, Zhang LH, Butters TD, Ye XS. Rational design and synthesis of highly potent pharmacological chaperones for treatment of N370S mutant Gaucher disease. J. Med. Chem. 2009; 52:3146–3149. [PubMed: 19397268]

31. Yu Z, Sawkar AR, Whalen LJ, Wong CH, Kelly JW. Isofagomine- and 2,5-anhydro-2,5-imino-D-glucitol-based glucocerebrosidase pharmacological chaperones for Gaucher disease intervention. J. Med. Chem. 2007; 50:94–100. [PubMed: 17201413]

32. Lei K, Ninomiya H, Suzuki M, Inoue T, Sawa M, Iida M, Ida H, Eto Y, Ogawa S, Ohno K, Suzuki Y. Enzyme enhancement activity of N-octyl-beta-valienamine on beta-glucosidase mutants associated with Gaucher disease. Biochim. Biophys. Acta. 2007; 1772:587–596. [PubMed: 17363227]

33. Lin H, Sugimoto Y, Ohsaki Y, Ninomiya H, Oka A, Taniguchi M, Ida H, Eto Y, Ogawa S, Matsuzaki Y, Sawa M, Inoue T, Higaki K, Nanba E, Ohno K, Suzuki Y. N-octyl-beta-valienamine up-regulates activity of F213I mutant beta-glucosidase in cultured cells: a potential chemical chaperone therapy for Gaucher disease. Biochim. Biophys. Acta. 2004; 1689:219–228. [PubMed: 15276648]

34. Sanchez-Olle G, Duque J, Egido-Gabas M, Casas J, Lluch M, Chabas A, Grinberg D, Vilageliu L. Promising results of the chaperone effect caused by imino sugars and aminocyclitol derivatives on mutant glucocerebrosidases causing Gaucher disease. Blood Cells Mol. Dis. 2009; 42:159–166. [PubMed: 19167250]

35. Diaz L, Casas J, Bujons J, Llebaria A, Delgado A. New glucocerebrosidase inhibitors by exploration of chemical diversity of N-substituted aminocyclitols using click chemistry and in situ screening. J. Med. Chem. 2011; 54:2069–2079. [PubMed: 21370884]

36. Trapero A, Alfonso I, Butters TD, Llebaria A. Polyhydroxylated bicyclic isoureas and guanidines are potent glucocerebrosidase inhibitors and nanomolar enzyme activity enhancers in Gaucher cells. J. Am. Chem. Soc. 2011; 133:5474–5484. [PubMed: 21413704]

37. Maegawa GH, Tropak MB, Buttner JD, Rigat BA, Fuller M, Pandit D, Tang L, Kornhaber GJ, Hamuro Y, Clarke JT, Mahuran DJ. Identification and characterization of ambroxol as an enzyme enhancement agent for Gaucher disease. J. Biol. Chem. 2009; 284:23502–23516. [PubMed: 19578116]

38. Marugan JJ, Zheng W, Motabar O, Southall N, Goldin E, Westbroek W, Stubblefield BK, Sidransky E, Aungst RA, Lea WA, Simeonov A, Leister W, Austin CP. Evaluation of quinazoline analogues as glucocerebrosidase inhibitors with chaperone activity. J Med. Chem. 2011; 54:1033–1058. [PubMed: 21250698]

39. Lieberman RL, Wustman BA, Huertas P, Powe AC Jr, Pine CW, Khanna R, Schlossmacher MG, Ringe D, Petsko GA. Structure of acid beta-glucosidase with pharmacological chaperone provides insight into Gaucher disease. Nat. Chem. Biol. 2007; 3:101–107. [PubMed: 17187079]

40. Khanna R, Benjamin ER, Pellegrino L, Schilling A, Rigat BA, Soska R, Nafar H, Ranes BE, Feng J, Lun Y, Powe AC, Palling DJ, Wustman BA, Schiffmann R, Mahuran DJ, Lockhart DJ, Valenzano KJ. The pharmacological chaperone isofagomine increases the activity of the Gaucher disease L444P mutant form of beta-glucosidase. FEBS J. 2010; 277:1618–1638. [PubMed: 20148966]

41. Steet RA, Chung S, Wustman B, Powe A, Do H, Kornfeld SA. The iminosugar isofagomine increases the activity of N370S mutant acid beta-glucosidase in Gaucher fibroblasts by several mechanisms. Proc. Natl. Acad. Sci. U.S.A. 2006; 103:13813–13818. [PubMed: 16945909]

42. http://www.amicustherapeutics.com/clinicaltrials

43. Sun Y, Ran H, Liou B, Quinn B, Zamzow M, Zhang W, Bielawski J, Kitatani K, Setchell KD, Hannun YA, Grabowski GA. Isofagomine in vivo effects in a neuronopathic Gaucher disease mouse. PLoS ONE. 2011; 6:e19037. [PubMed: 21533102]

44. Paulsen H, Todt K. On monosaccharides with nitrogen-yielding seven membered rings. Chem. Ber. 1967; 100:512–520. [PubMed: 5594777]
45. Painter GF, Eldridge PJ, Falshaw A. Syntheses of tetrahydroxyazepanes from chiro-inositols and their evaluation as glycosidase inhibitors. Bioorg. Med. Chem. 2004; 12:225–232. [PubMed: 14697787]
46. Qian X, Moris-Varas F, Fitzgerald MC, Wong CH. C2-symmetrical tetrahydroxyazepanes as inhibitors of glycosidases and HIV/FIV proteases. Bioorg. Med. Chem. 1996; 4:2055–2069. [PubMed: 9022971]
47. Moris-Varas F, Qian X, Wong CH. Enzymatic/chemical synthesis and biological evaluation of seven-membered iminocyclitols. J. Am. Chem. Soc. 1996; 118:7647–7652.
48. Markad SD, Karanjule NS, Sharma T, Sabharwal SG, Dhavale DD. Polyhydroxylated homoazepanes and 1-deoxy-homonojirimycin analogues: Synthesis and glycosidase inhibition study. Org. Biomol. Chem. 2006; 4:3675–3680. [PubMed: 16990944]
49. Li H, Bleriot Y, Chantereau C, Mallet JM, Sollogoub M, Zhang Y, Rodriguez-Garcia E, Vogel P, Jimenez-Barbero J, Sinay P. The first synthesis of substituted azepanes mimicking monosaccharides: a new class of potent glycosidase inhibitors. Org. Biomol. Chem. 2004; 2:1492–1499. [PubMed: 15136805]
50. Shih TL, Liang MT, Wu KD, Lin CH. Synthesis of polyhydroxy 7- and N-alkyl-azepanes as potent glycosidase inhibitors. Carbohydr. Res. 2011; 346:183–190. [PubMed: 21146809]
51. Li H, Liu T, Zhang Y, Favre S, Bello C, Vogel P, Butters TD, Oikonomakos NG, Marrot J, Bleriot Y. New synthetic seven-membered 1-azasugars displaying potent inhibition towards glycosidases and glucosylceramide transferase. Chembiochem. 2008; 9:253–260. [PubMed: 18188862]
52. Butters TD, Alonzi DS, Kukushkin NV, Ren Y, Bleriot Y. Novel mannosidase inhibitors probe glycoprotein degradation pathways in cells. Glycoconj. J. 2009; 26:1109–1116. [PubMed: 19234785]
53. Marcelo F, He Y, Yuzwa SA, Nieto L, Jimenez-Barbero J, Sollogoub M, Vocadlo DJ, Davies GD, Bleriot Y. Molecular basis for inhibition of GH84 glycoside hydrolases by substituted azepanes: conformational flexibility enables probing of substrate distortion. J. Am. Chem. Soc. 2009; 131:5390–5392. [PubMed: 19331390]
54. Xiao X, Bai D. An efficient and selective method for hydrolysis of acedonides. Synlett. 2001; 4:535–537.
55. Lohray BB, Jayamma Y, Chatterjee M. Unprecedented selectivity in the reaction of 1,2:5,6-Dianhydro-3,4-O- isopropylidenehexitols with benzylamine: a practical synthesis of 3,4,5,6-tetrahydroxyazepanes. J. Org. Chem. 1995; 60:5958–5960.
56. Bradford MM. A rapid and sensitive method for the quantitation of microgram quantities of protein utilizing the principle of protein-dye binding. Anal. Biochem. 1976; 72:248–254. [PubMed: 942051]
57. Orwig SD, Lieberman RL. Biophysical characterization of the olfactomedin domain of myocilin, an extracellular matrix protein implicated in inherited forms of glaucoma. PLoS ONE. 2011; 6:e16347. [PubMed: 21283635]
58. Otwinowski Z, Minor W. Processing of X-ray diffraction data collected in oscillation mode. Methods Enzymol. 1997; 276:307–326.
59. Collaborative Computational Project, Number 4. The CCP4 Suite: Programs for Protein Crystallography. Acta Crystallogr. 1994; D50:760.
60. Emsley P, Lohkamp B, Scott WG, Cowtan K. Features and development of Coot. Acta Crystallogr. 2010; D66:486–501.
61. Schuttelkopf AW, van Aalten DM. PRODRG: a tool for high-throughput crystallography of protein-ligand complexes. Acta Crystallogr. 2004; D60:1355–1363.
62. DeLano, WL. The PyMOL Molecular Graphics System. San Carlos, CA: DeLano Scientific; 2002.
63. Sawkar AR, Adamski-Werner SL, Cheng WC, Wong CH, Beutler E, Zimmer KP, Kelly JW. Gaucher disease-associated glucocerebrosidases show mutation-dependent chemical chaperoning profiles. Chem. Biol. 2005; 12:1235–1244. [PubMed: 16298303]
64. Gloster TM, Davies GJ. Glycosidase inhibition: assessing mimicry of the transition state. Org. Biomol. Chem. 2010; 8:305–320. [PubMed: 20066263]

65. Aguilar-Moncayo M, Gloster TM, Turkenburg JP, Garcia-Moreno MI, Ortiz Mellet C, Davies GJ, Garcia Fernandez JM. Glycosidase inhibition by ring-modified castanospermine analogues: tackling enzyme selectivity by inhibitor tailoring. Org. Biomol. Chem. 2009; 7:2738–2747. [PubMed: 19532990]
66. Strasberg PM, Lowden JA. The assay of glucocerebrosidase activity using the natural substrate. Clin. Chim. Acta. 1982; 118:9–20. [PubMed: 7053909]
67. Yu L, Ikeda K, Kato A, Adachi I, Godin G, Compain P, Martin O, Asano N. Alpha-1-C-octyl-1-deoxynojirimycin as a pharmacological chaperone for Gaucher disease. Bioorg. Med. Chem. 2006; 14:7736–7744. [PubMed: 16919960]
68. Lieberman RL, D'aquino JA, Ringe D, Petsko GA. The effects of pH and iminosugar pharmacological chaperones on lysosomal glycosidase structure and stability. Biochemistry. 2009; 48:4816–4827. [PubMed: 19374450]
69. Lieberman RL. A guided tour of the structural biology of Gaucher disease: acid-beta-glucosidase and saposin C. Enzyme Res. 2011 *in press*.
70. Brumshtein B, Greenblatt HM, Butters TD, Shaaltiel Y, Aviezer D, Silman I, Futerman AH, Sussman JL. Crystal structures of complexes of N-butyl- and N-nonyl-deoxynojirimycin bound to acid beta-glucosidase: insights into the mechanism of chemical chaperone action in Gaucher disease. J. Biol. Chem. 2007; 282:29052–29058. [PubMed: 17666401]
71. Dvir H, Harel M, McCarthy AA, Toker L, Silman I, Futerman AH, Sussman JL. X-ray structure of human acid-beta-glucosidase, the defective enzyme in Gaucher disease. EMBO Rep. 2003; 4:704–709. [PubMed: 12792654]
72. Miao S, McCarter JD, Grace ME, Grabowski GA, Aebersold R, Withers SG. Identification of Glu340 as the active-site nucleophile in human glucocerebrosidase by use of electrospray tandem mass spectrometry. J. Biol. Chem. 1994; 269:10975–10978. [PubMed: 7908905]
73. Premkumar L, Sawkar AR, Boldin-Adamsky S, Toker L, Silman I, Kelly JW, Futerman AH, Sussman JL. X-ray structure of human acid-beta-glucosidase covalently bound to conduritol-B-epoxide. Implications for Gaucher disease. J. Biol. Chem. 2005; 280:23815–23819. [PubMed: 15817452]
74. Wei RR, Hughes H, Boucher S, Bird JJ, Guziewicz N, Van Patten SM, Qiu H, Pan CQ, Edmunds T. X-ray and biochemical analysis of N370S mutant human acid beta-glucosidase. J. Biol. Chem. 2011; 286:299–308. [PubMed: 20980263]
75. Leinekugel P, Michel S, Conzelmann E, Sandhoff K. Quantitative correlation between the residual activity of beta-hexosaminidase A and arylsulfatase A and the severity of the resulting lysosomal storage disease. Hum. Genet. 1992; 88:513–523. [PubMed: 1348043]
76. Desnick, RJ.; Fan, JQ. Pharmacologic chaperone therapy for lysosomal diseases, In. In: Futerman, AH.; Zimran, A., editors. Gaucher Disease. Boca Raton: CRC Press; 2006. p. 377-397.

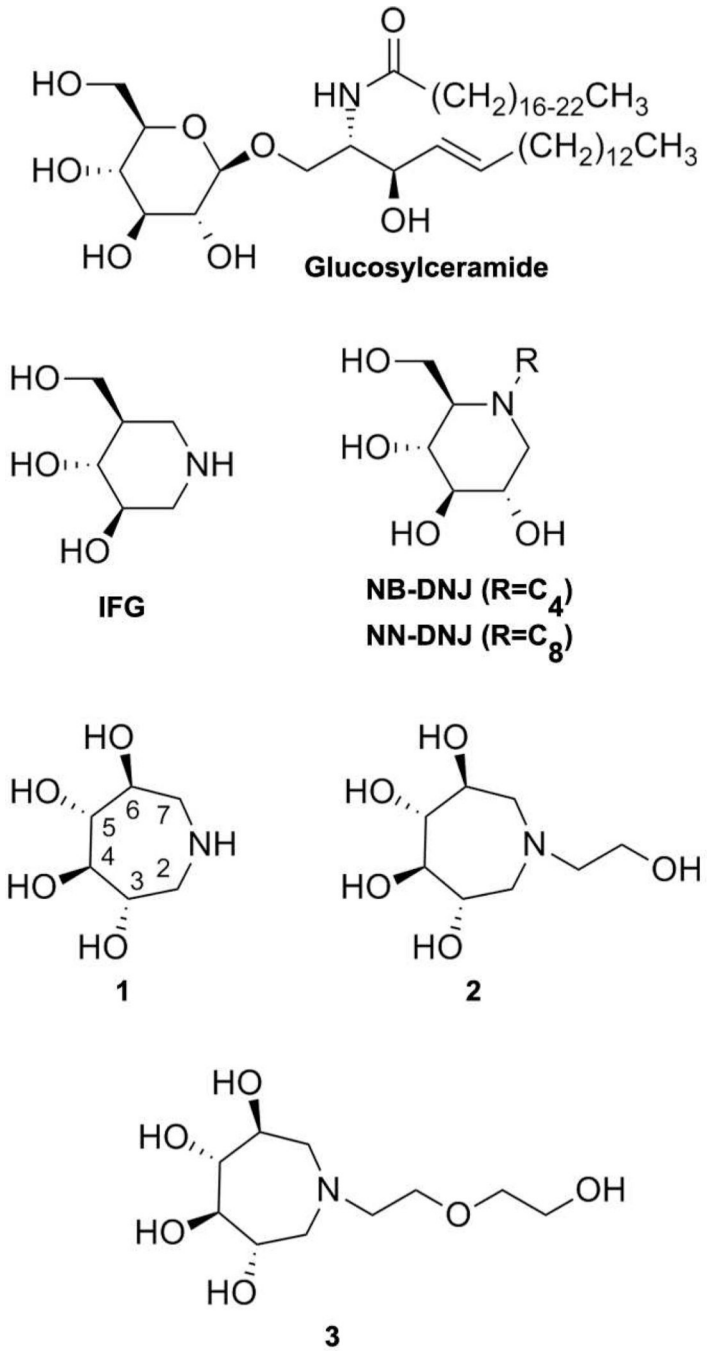

Fig. 1.

Chemical structure of the natural GCase substrate, GlcCer, representative azasugars investigated as pharmacologic chaperones, IFG, NB- and NN- DNJs, as well as the azepane compounds **1**, **2**, and **3** described in this study.

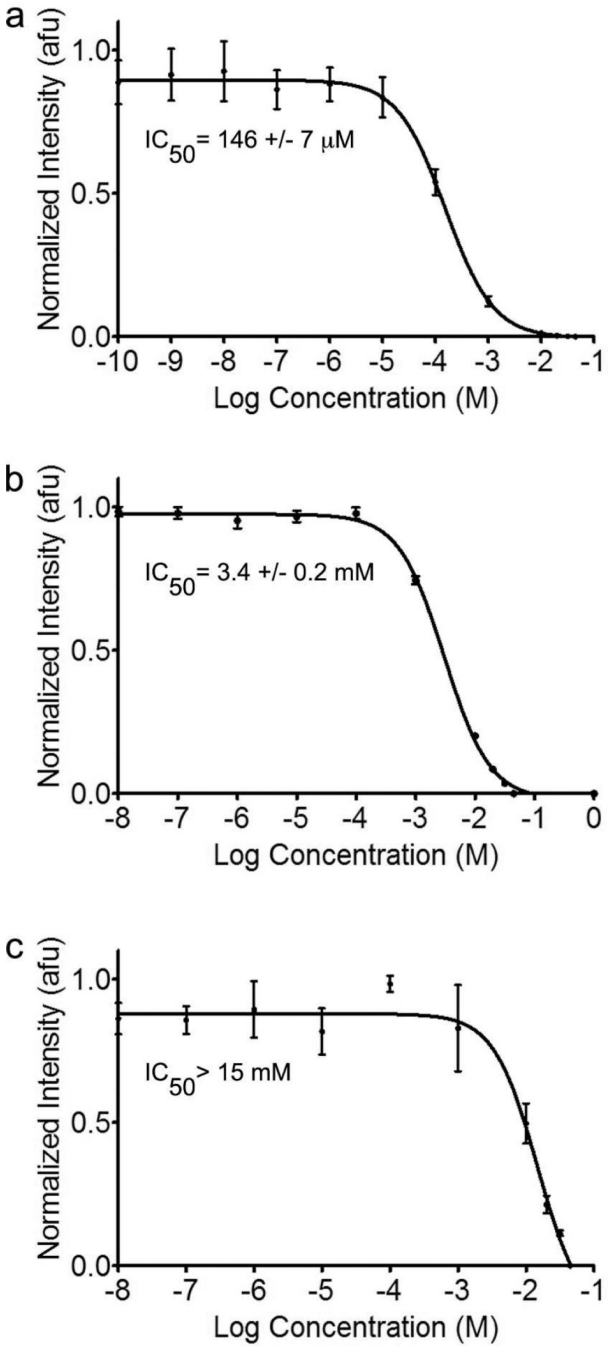

Fig. 2.

Competitive inhibition curves for **1**, **2**, and **3**, respectively, toward GCase. Inset: IC_{50} values. Error bars indicate standard deviation.

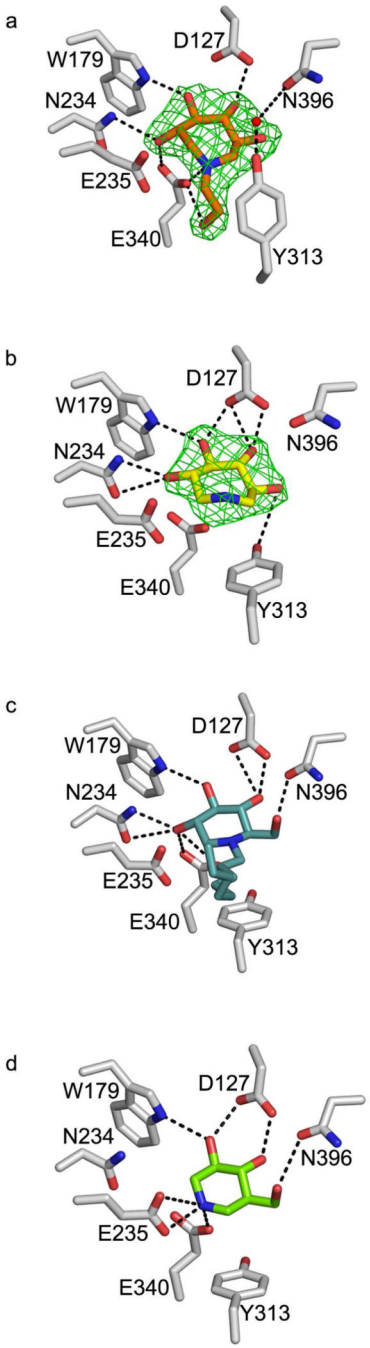

Fig. 3.

Ball-and-stick representation of the GCase active site upon compound binding. (A) **2** (B) **1** (C) NN-DNJ (PDB code 2V3E) (D) IFG (PDB code 2NSX). Difference (F_o— F_c) electron density for 1 and 2 was calculated from the initial phasing solution using only protein coordinates and is contoured to 3σ. Hydrogen bonding interactions are indicated by dashed black lines and represent distances between 2.5 Å– 3.5 Å.

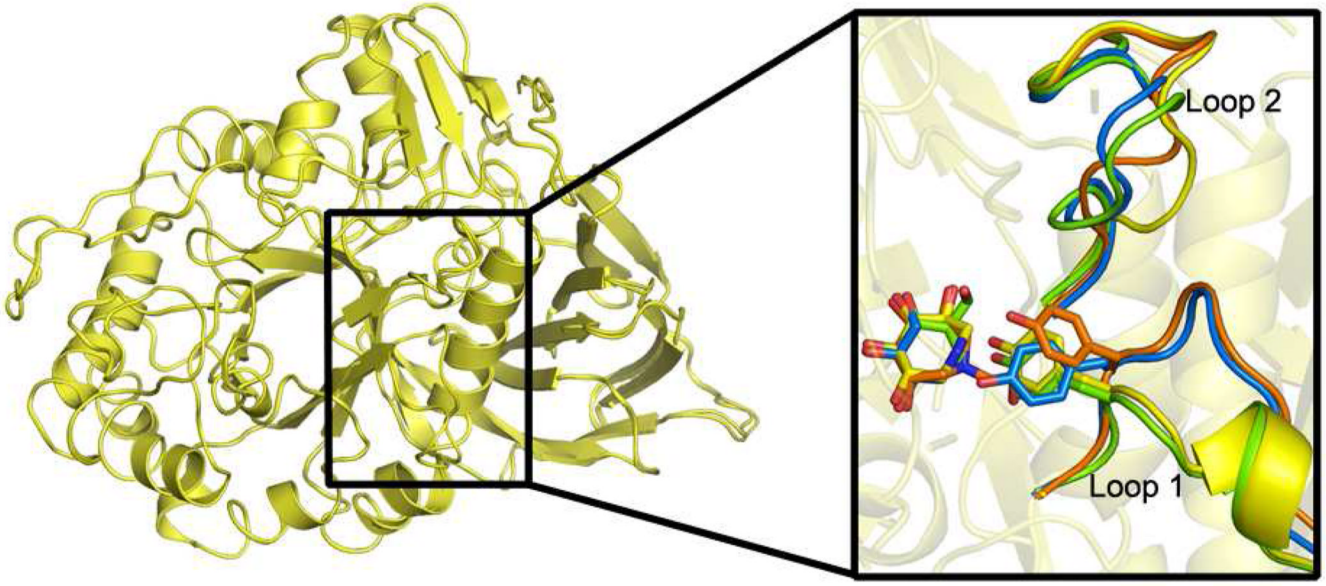

Fig. 4.

Superposition of **1** and **2** bound GCase structures and comparison of loops adjacent to the active site (inset). After binding, Loop 1 adopts either a helical turn as seen for compound 1 (inset, yellow) and IFG (inset, green), or an extended loop conformation seen in the compound 2 (inset, orange) and glycerol (inset, blue) bound structures. Changes in Loop 2 are due to crystal packing (see text).

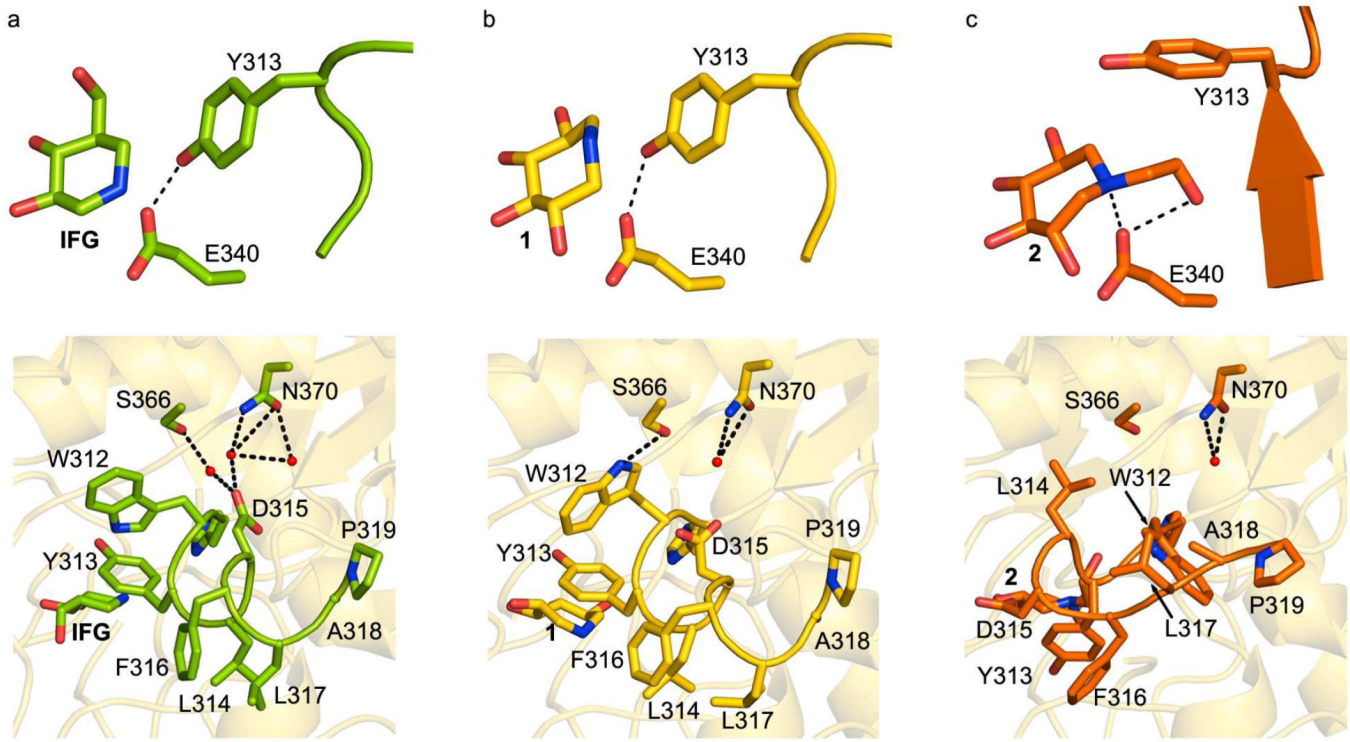

Fig. 5.

Comparison of Loop 1 configuration. (A) IFG-, (B) 1-, and (C) 2- bound GCase. Top: orientation of Tyr 313 relative to Glu 340. Bottom: interactions of loop with interior GCase helix harboring Asn 370. Hydrogen bonding interactions are indicated by dashed black lines.

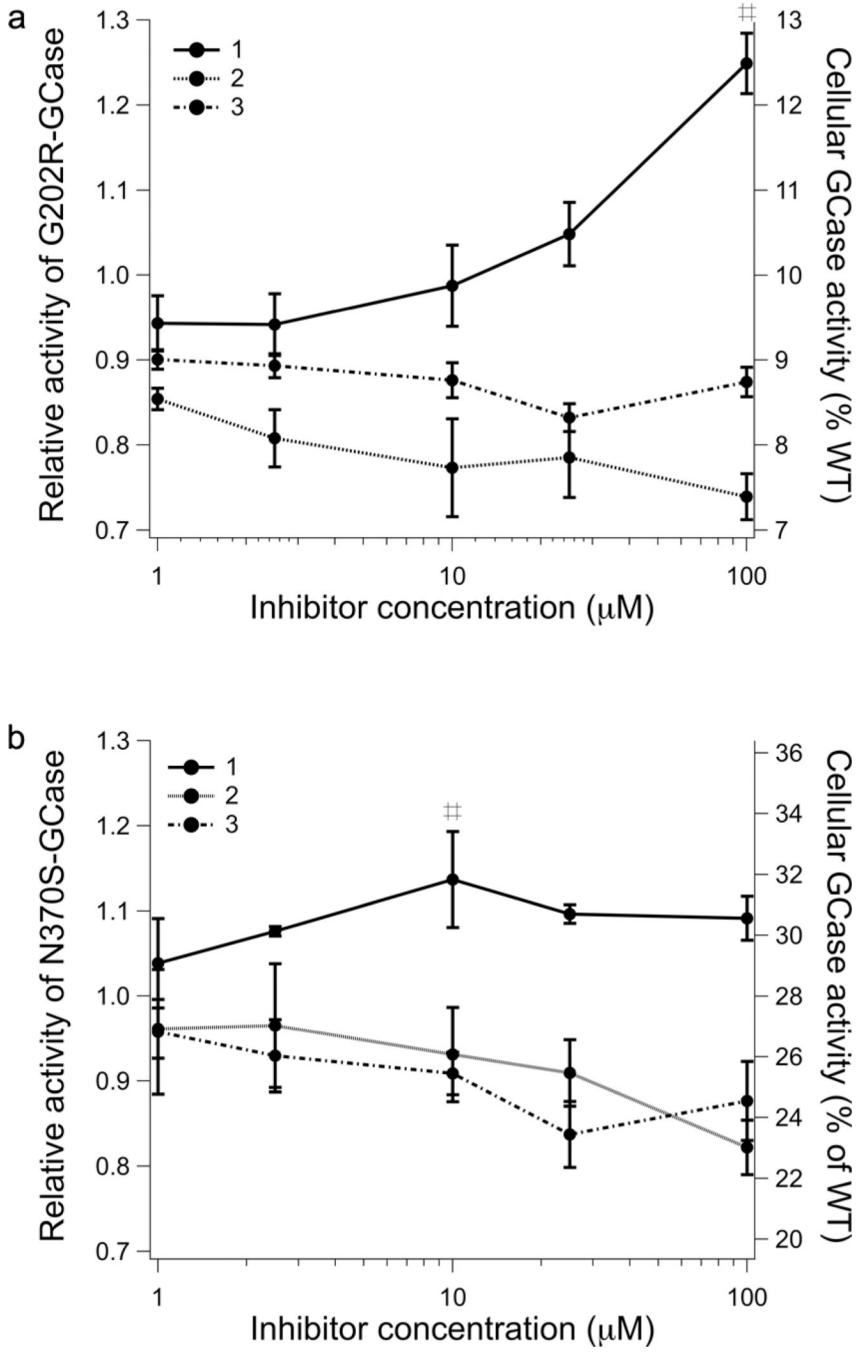

Fig. 6.

Effects of 1, 2, and 3 on mutant GCase activity in intact patient derived fibroblasts G202R (A) and N370S/V394L (B). Enzyme activity is normalized to untreated and assigned a relative activity of 1. The right-hand axis is the residual activity of the mutant expressed as the percentage of WT GCase activity. Mean values for triplicate experiments are shown. # = $p < 0.05$.

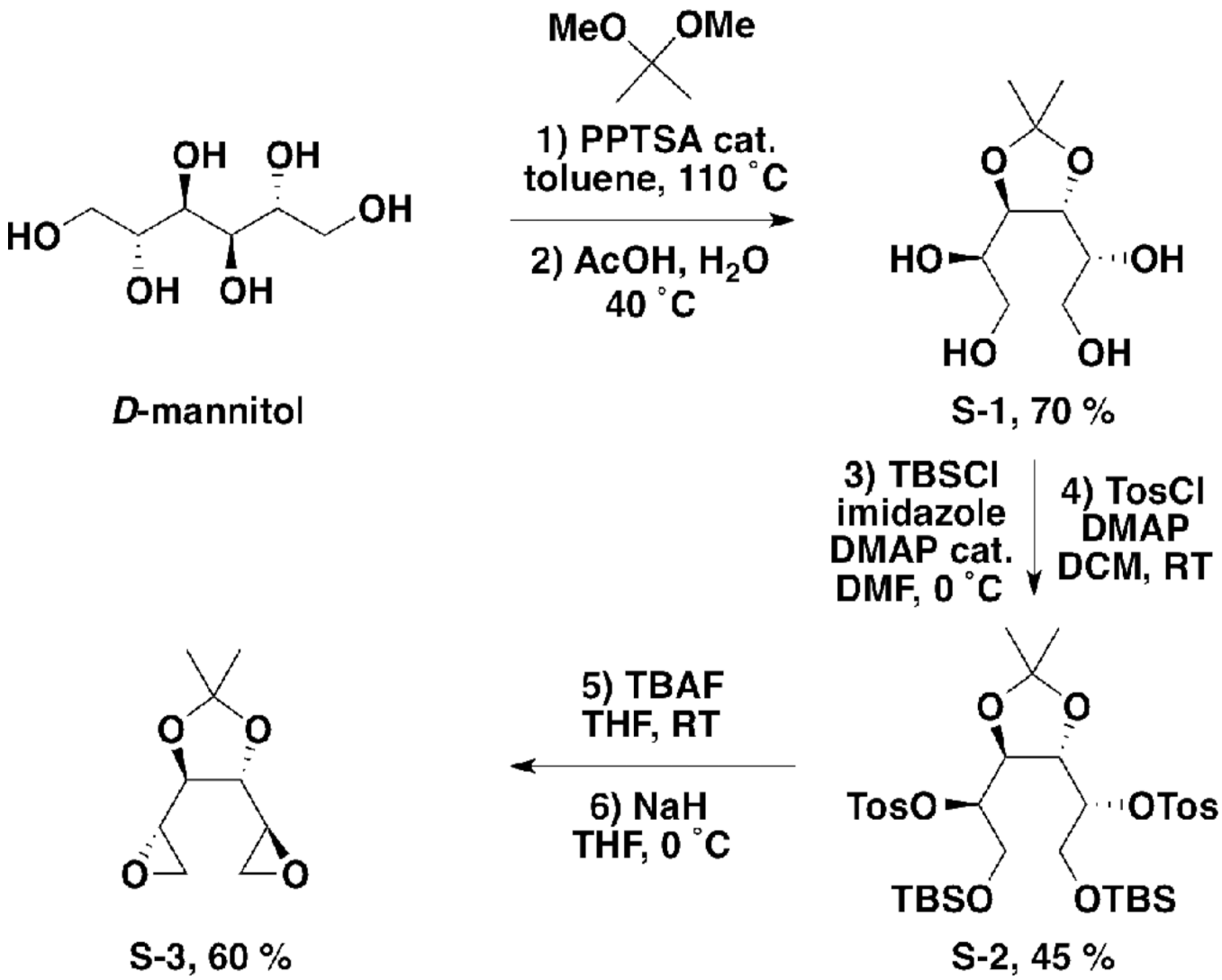

Scheme 1.
Synthesis of Di-epoxide **S-3**

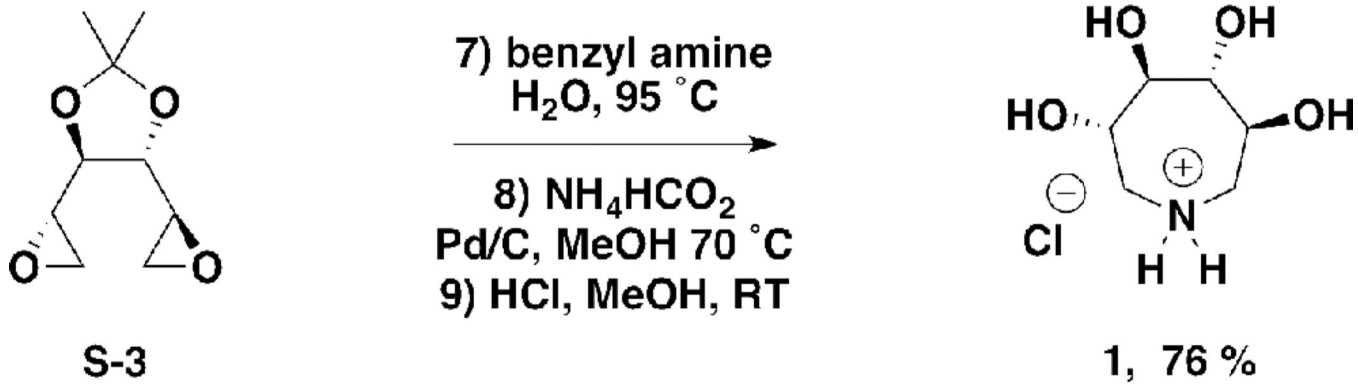

Scheme 2.
Synthesis of Tetrahydroxyazepane **1**

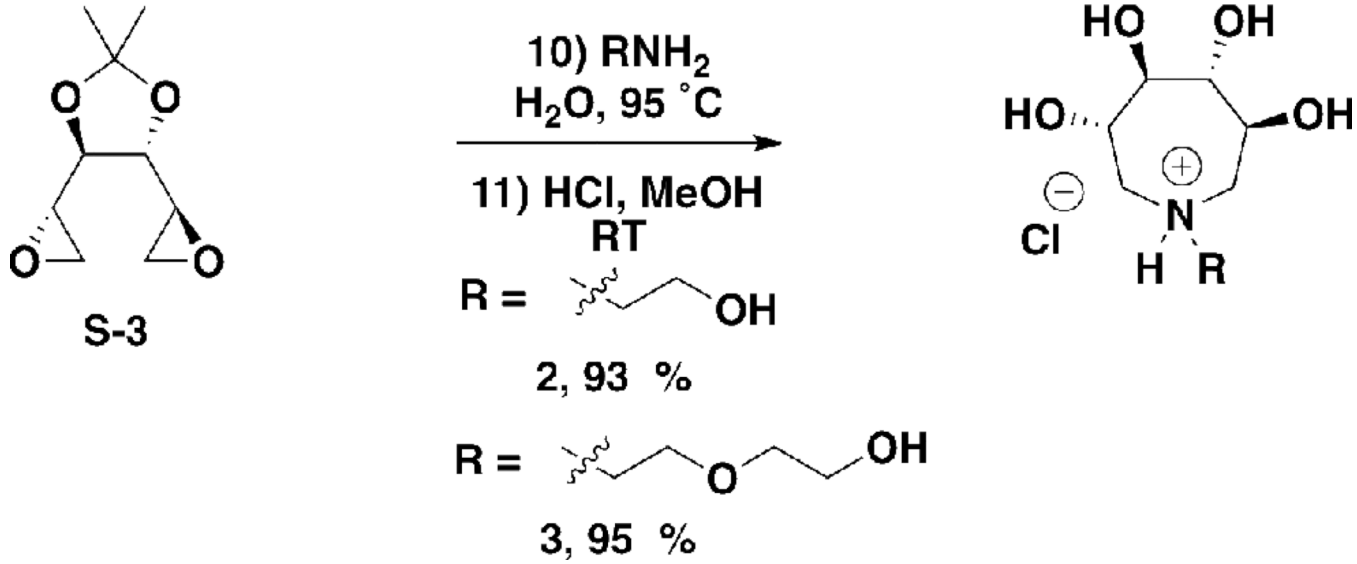

Scheme 3.
Synthesis of Tetrahydroxyazepanes **2** and **3**

Table 1

Data collection and refinement statistics.

	3RIL (1)	**3RIK (2)**
Data Statistics		
space group	P2(1)	P2(1)
Cell dimensions		
a, *b*, *c* (Å)	109.2, 91.4, 152.7	108.0, 91.6, 152.2
α, β, γ (deg)	90.0, 110.95, 90.0	90.0, 110.70, 90.0
Resolution (Å)[a]	44.5-2.4 (2.49-2.40)	46.5-2.5 (2.55-2.48)
R_{sym}[a]	10.5 (35.7)	12.2 (47.8)
%>3σ[a]	62.9 (38.3)	64.6 (40.7)
Completeness (%)[a]	96.3 (76.5)	94.3 (72.3)
redundancy	2.6	2.9
Refinement Statistics		
resolution (Å)	44.5-2.4	47-2.5
no. of reflections	100648 (5857)	88126 (4973)
R_{work}/R_{free}[a]	20.79/24.9	18.1/23.4
no. of molecules		
protein molecules in asymmetric unit	4	4
protein residues	1988	1988
N-acetylglucosamine (NAG)	4	4
sulfate anion (SO_4^{2-})	7	7
chaperone	4	2
water	1254	702
B-factor (Å^2)		
protein	23.6	26.6
NAG	29.7	50.4
SO_4^{2-}	60.8	38.1
chaperone	38.2	32.9
water	27.6	40.0
rmsd		
bond lengths (Å)	0.006	0.013
bond lengths (deg)	1.089	1.466

[a] Data for the highest-resolution shell given in parenthesis; 5% or reflections were selected for R_{free}.

Table 2

Stabilization of GCase with inhibitors at acidic and neutral pH.

		1		2		3		IFG	
	Inhibitor (mM)	**T_m(°C)**	**ΔT_m**	**T_m(°C)**	**ΔT_m**	**T_m(°C)**	**ΔT_m**	**T_m(°C)**	**ΔT_m**
pH 5.2		55.8 ± 0.0[a]							
	0.5	56.4 ± 0.0	0.6	55.9 ± 0.1	0.3	56.1 ± 0.0	0.3	68.0 ± 0.2	12.2
	1	56.6 ± 0.0	0.8	56.0 ± 0.0	0.3	56.1 ± 0.1	0.2	68.9 ± 0.3	13.0
	2	57.3 ± 0.1	1.5	56.7 ± 0.1	1.0	56.7 ± 0.1	0.8	69.7 ± 0.3	13.8
	5	58.4 ± 0.1	2.7	57.4 ± 0.1	1.7	57.2 ± 0.1	1.3	67.5 ± 0.3	11.6
	10	59.0 ± 0.1	3.2	57.4 ± 0.0	1.7	56.9 ± 0.0	1.0	63.7 ± 0.2	7.8
pH 7.2		47.1 ± 0.2 [a]							
	0.5	48.5 ± 0.1	1.4	48.7 ± 0.1	1.7	50.7 ± 0.0	2.1	63.8 ± 0.3	16.9
	1	49.4 ± 0.1	2.3	49.3 ± 0.0	2.2	52.0 ± 0.1	3.3	65.4 ± 0.1	18.4
	2	49.9 ± 0.1	2.8	50.1 ± 0.1	3.1	52.6 ± 0.1	3.9	67.2 ± 0.2	20.2
	5	52.5 ± 0.1	5.4	52.1 ± 0.1	5.0	53.6 ± 0.1	5.0	70.3 ± 0.2	23.4
	10	54.6 ± 0.1	7.5	53.6 ± 0.1	6.5	54.5 ± 0.0	5.8	72.6 ± 0.2	25.7

[a] mean T_m measured for GCase at indicated pH value in the absence of inhibitor.

Biochemistry. Author manuscript; available in PMC 2012 December 13.